Journal of Applied Polymer Science

Influence of the nanofiber dimensions on the properties of nanocellulose/poly(vinyl alcohol) aerogels

Silvana Mueller,[1] Janak Sapkota,[1] Apiradee Nicharat,[1] Tanja Zimmermann,[2] Philippe Tingaut,[2] Christoph Weder,[1] E. Johan Foster[1,3]

[1]Adolphe Merkle Institute, University of Fribourg, Chemin des Verdiers 4, CH-1700 Fribourg, Switzerland

[2]Swiss Federal Laboratories for Materials Science and Technology, Laboratory for Applied Wood Materials, Überlandstrasse 129, Dübendorf CH-8600, Switzerland

[3]Virginia Tech, Department of Materials Science & Engineering, Blacksburg Virginia 24061

Correspondence to: C. Weder (E-mail: christoph.weder@unifr.ch) and E. J. Foster (E-mail: johanf@vt.edu)

ABSTRACT: The investigation of aerogels made from cellulose nanofibers and poly(vinyl alcohol) (PVOH) as a polymeric binder is reported. Aerogels based on different nanocellulose types were studied to investigate the influence of the nanocellulose dimensions and their rigidity on the morphology and mechanical properties of the resulting aerogels. Thus, cellulose nanocrystals (CNCs) with low (10), medium (25), and high (80) aspect ratios, isolated from cotton, banana plants, and tunicates, respectively, microfibrillated cellulose (MFC) and microcrystalline cellulose (MCC) were dispersed in aqueous PVOH solutions and aerogels were prepared by freeze-drying. In addition to the cellulose type, the PVOH- and the CNC-concentration as well as the freeze-drying conditions were varied, and the materials were optionally cross-linked by an annealing step or the use of a chemical cross-linker. The data reveal that at low PVOH content, rigid, high-aspect ratio CNCs isolated from tunicates afford aerogels that show the least amount of shrinking upon freeze-drying and display the best mechanical properties. However, with increasing concentration of PVOH or upon introduction of a chemical cross-linker the differences between materials made from different nanocellulose types decrease. © 2014 Wiley Periodicals, Inc. J. Appl. Polym. Sci. **2015**, *132*, 41740.

KEYWORDS: biopolymers and renewable polymers; cellulose and other wood products; foams; nanoparticles; nanocrystals; structure-property relations

Received 29 September 2014; accepted 4 November 2014

DOI: 10.1002/app.41740

INTRODUCTION

Their renewable nature, biodegradability, low toxicity, high strength, and stiffness, and an abundance of reactive, readily modifiable surface hydroxyl groups, render cellulose nanofibers an attractive basis for a broad range of functional nanomaterials, including nanocomposites with polymers, barrier films, sorbents, just to name a few.[1–12] On account of their high-aspect ratio and large specific surface area, aqueous suspensions of cellulose nanofibers can easily be converted to hydrogels,[13–15] which in turn can be converted into aerogels with high porosity and low density by lyophilization or supercritical drying, optionally after including a polymeric binder, cross-linking agent, and/or other auxiliary components.[16] Modification of the surface hydroxyl groups has permitted the preparation of nanocellulose aerogels that appear to be useful as catalyst support,[17] in electrical devices,[18,19] oil-spill sorbents,[9–11,20,21] magnetically active devices,[22–24] and biomedical applications.[25–27] The aerogels in the aforementioned and many other studies were prepared from different nanocellulose types, including microfibrillated cellulose (MFC),[13,28–30] bacterial cellulose,[26,31–33] microcrystalline cellulose (MCC),[34–36] and cellulose nanocrystals (CNCs).[14,37,38] The materials reported were made by different procedures, varied in composition,[28–30,39] and the influence of different polymeric binders was explored.[37,40–42] As the materials reported in previous studies differ usually in more than one design parameter, it is difficult to extract from the available data how the nature of the nanocellulose, and more specifically the aspect ratio of the nanofibers, influences the aerogel's properties. It is well known that the reinforcement effect of CNCs in polymer nanocomposites[1] depends not only on the CNC-concentration in the polymeric matrix, but also increases with the aspect ratio[43,44] and the on-axis stiffness of the filler.[45] It has also been reported that the stiffness of solution-cast nanocellulose films scales with the CNC's aspect ratio.[43,44] Thus, one can speculate that also the properties of nanocellulose aerogels are

Additional Supporting Information may be found in the online version of this article.

influenced by the aspect ratio of their building blocks. We here report a systematic study in which this relationship was investigated and the key parameter varied was the aspect ratio and the elastic modulus of the nanocellulose. In a comparative manner, we also explored how the variation of other factors such as the concentration of the nanocellulose and the polymeric binder, the freezing conditions prior to lyophilization and optional cross-linking by an annealing step or use of a chemical cross-linker influenced this relationship.

As a test bed, we utilized a recently reported framework for the preparation of water-insoluble aerogels made by lyophilization of aqueous mixtures containing CNCs extracted from cotton and poly(vinyl alcohol) (PVOH) as a binder.[46] We previously varied the PVOH and the CNC concentration as well as the freezing conditions prior to lyophilization and the effect of these parameters on the morphology, specific surface area, and mechanical properties of the resulting aerogels was explored. Our initial results revealed that in the case of low-aspect ratio CNCs isolated from cotton, the PVOH concentration in the aqueous mixture was the most important parameter that influenced the compressive Young's modulus of the aerogels made, while the CNC concentration did not cause major changes. As already observed by Dash *et al.*[47] and Zhou *et al.*,[48] we also found that the pore morphology was affected by freezing speed and the CNC concentration and that slower freezing at higher temperature afforded more coherent materials than fast freezing (FF) at lower temperature. Finally, we demonstrated that an isothermal annealing process can be used to impart a certain degree of cross-linking, which was concomitant with a higher stiffness and a reduced water dispersibility of the annealed materials.[46] A higher stiffness was also achieved by chemical cross-linking with sodium tetraborate (borax, $Na_2B_4O_7$), although the corresponding aerogels did not exhibit a significantly reduced water dispersibility, on account of the reversibility of the cross-linking reaction.[49,50]

We now extended our investigation to materials prepared with CNCs that we isolated from different sources. To cover a broad range of aspect ratios, high-aspect ratio CNCs isolated by sulfuric acid hydrolysis from the mantles of tunicates (t-CNCs, l = 1798 ± 527 nm, d = 25 ± 7 nm, A = 73), intermediate-aspect ratio CNCs derived from the pseudostem of banana plants (b-CNCs, l = 412 ± 119 nm, d = 17 ± 5 nm, A = 24), and low-aspect ratio CNCs derived from microcrystalline cellulose (m-CNCs, l = 277 ± 61 nm, d = 24 ± 7 nm, A = 11) were used. We also studied the corresponding aerogels based on MFC (d = 25 ± 8 nm),[51] which consists of cellulose nanofibers that have a length of several μm (and the aspect ratio is difficult to determine), and included our previously reported data for aerogels based on CNCs derived from cotton (c-CNCs, l = 160 - 300 nm, d = 10–24 nm, A = 11 nm).[46]

We note that the different CNCs used not only vary in dimensions, but also in crystallinity, strength, and stiffness. For example the elastic modulus of CNCs is reported as 105 GPa for CNCs extracted from cotton[52] and 143 GPa for CNCs extracted from tunicates,[53] whereas the elastic modulus and the apparent crystallinity of MFC, typically between 40 and 70 GPa[3] and around 60%,[54] respectively, are much lower compared with CNCs (59–96%).[55–57]

EXPERIMENTAL

Materials and General Methods

Sulfuric acid, 95–97%, for analysis, Reag. ISO, Reag. Ph. Eur. was purchased from Honeywell Chemicals. Sodium hydroxide (reagent grade pellets, anhydrous, ≥ 98%), acetic acid (Reagent plus®, ≥99%), hydrogen peroxide solution (35% w/w in H_2O), PVOH (weight-average molecular weight M_W = 85,000-124,000, 99+% hydrolyzed) and sodium tetraborate decahydrate ($Na_2B_4O_7 \cdot 10\ H_2O$, Reagent plus® ≥99.5%) were purchased from Sigma Aldrich Switzerland. All chemicals were used without any further purification. Sonication was done in a SONO SWISS SW 3H sonicator with a power of 280 W, heating was done in a BINDER oven, freezing was done in a Liebherr Premium Freezer operating at −26°C. Purified water from a milliQ Sartorius arium 611VF water purifying system was used.

Preparation of Nanocelluloses

CNCs extracted from the stem of banana plants (b-CNCs, l = 412 ± 119 nm, d = 17 ± 5 nm, A = 24) were extracted from the pseudostems of the species *musa sapientum linn* following a reported protocol.[58] CNCs derived from tunicates (t-CNCs, l = 1798 ± 527 nm, d = 25 ± 7 nm, A = 73) were extracted from exemplars of the species *styela clava*, sessile sea creatures, collected from floating docks at Port de Plaisance du Moulin Blanc, France, following the protocol of Favier *et al.*[1] and applying the same modifications as reported by Shanmuganathan *et al.*[59] Lattice NT microcrystalline cellulose (MCC) with an average particle size of 108 μm was purchased from FMC Biopolymer. As discussed below, this material was disintegrated *in situ* to form m-CNCs. MFC (diameter: 24 ± 9 nm) was prepared from elemental chlorine free (ECF) bleached softwood pulp fibers by mechanical disintegration using a Masuko-grinder as previously described by Josset *et al.*[60] Fiber slurries of 2% dry weight content were swollen in water for 24 h and then passed 10 times through the rotating stones (1500 rpm) of the grinder.

Preparation of b-CNC Aerogels

Aerogels made from b-CNCs were prepared according to our recently published protocol.[46] PVOH solutions were prepared by dissolving appropriate amounts of PVOH in H_2O at 90°C (30 min for [PVOH] = 10 mg/mL, 2 h for [PVOH] = 20 mg/mL, 12 h for [PVOH] = 40 mg/mL). Lyophilized b-CNCs were added to the aqueous PVOH solutions and dispersed by sonicating the mixtures for 8 h. The b-CNC-concentration was varied between 20 and 100 mg/mL, while the PVOH concentration was set between 10 and 40 mg/mL. After sonication, the b-CNC/PVOH mixtures were transferred into glass vials with an outer diameter of 18 mm and then frozen. Two different freezing procedures were employed: the CNC/PVOH mixtures were either immersed for 5 min in liquid nitrogen at −196°C (this method is referred to as "fast freezing/FF") or stored in a freezer at −26°C for 24 h (this method is referred to as "slow freezing/SF"). The ice was then sublimed by lyophilization for at least 48 h, before the vials were broken to remove well-defined, cylindrical aerogels with a diameter of approximately 14 mm.

Preparation of t-CNC Aerogels

The preparation of aerogels from t-CNCs largely followed the process applied for b-CNCs, but due to the high viscosity, the initial mixtures prepared had a lower solid content. Thus, lyophilized t-CNCs were dispersed in the aqueous PVOH solutions by a cycle of vigorous stirring for 1 h that was followed by 2 h of sonication. Repeating these two steps about six times led to a good dispersion of the t-CNCs. The initial CNC concentration was varied between 8 and 10 mg/mL and the PVOH-concentration, depending on the targeted solid content, between 2 mg/mL and 8 mg/mL. To prepare suspensions with the same CNC concentrations as for the other aerogels, water was removed from these mixtures by controlled evaporation. Thus, measured volumes of t-CNC/PVOH mixtures were transferred into a beaker, which was covered with a perforated aluminum foil. The beakers were stored in an oven at 70°C under ambient pressure until the amount of evaporated H_2O (determined by volumetric analysis) matched with the targeted solid content. The viscous mixtures were transferred into glass vials and cylindrical aerogels with a diameter of approximately 14 mm were prepared in analogy to the b-CNC aerogels.

Preparation of MFC Aerogels

Aqueous dispersions with an MFC concentration of between 20 and 100 mg/mL and a PVOH concentration of between 10 mg/mL and 40 mg/mL were prepared by vigorously stirring aqueous mixtures containing appropriate amounts of lyophilized MFC in corresponding PVOH solutions for at least 12 h. The MFC/PVOH mixtures were transferred into glass vials and cylindrical aerogels with a diameter of approximately 13 mm were prepared in analogy to the b-CNC aerogels.

Preparation of MCC Aerogels

Aqueous dispersions with an MCC concentration of between 20 and 100 mg/mL and a PVOH concentration of between 10 mg/mL and 40 mg/mL were prepared by stirring aqueous mixtures containing appropriate amounts of lyophilized MCC in corresponding PVOH solutions for 6 h, subsequently sonicating for 12 h, and again stirring for 1 h. The MCC/PVOH mixtures were transferred into glass vials and cylindrical aerogels with a diameter of approximately 12 mm were prepared in analogy to the b-CNC aerogels.

Cross-Linking of Aerogels

Thermal and chemical cross-linking of aerogels was achieved as previously reported.[46] Briefly, thermal cross-linking involved annealing lyophilized aerogels at 150°C for 60 min. Chemical cross-linking was accomplished by adding aqueous $Na_2B_4O_7$ solutions with a concentration of 0.1 M to the cellulose/PVOH dispersions with a volume ratio of 1 : 4. The cross-linking was ensured by vigorously stirring the mixture and subsequently storing the vials at 45°C for 12 h. Then the solvent was frozen at −26°C for 24 h and removed by lyophilization.

Scanning Electron Microscopy

Scanning electron microscopy (SEM) images were acquired on a FEI XL 30 Sirion FEG microscope. The microscope was operated with an acceleration voltage of 20 kV and all micrographs were recorded using the secondary electron mode. All samples were fractured at ambient temperature and pressure, and then fixed on the sample holder with double-sided carbon tapes. The conductivity of the samples was increased by painting the vertical sides of the samples with silver paint. The surface of the samples, which was always the inner part of the samples that was revealed after fractioning, were coated with Au in a Baltec MED 020 coating system with a layer thickness of 40 nm.

Transmission Electron Microscopy

Transmission electron microscopy (TEM) was carried out to probe the structure of the different nanocelluloses. Thus, the lyophilized CNCs were dispersed in H_2O as follows. CNC-suspensions were sonicated for 4 h (c-CNCs), 8 h (b-CNCs) and 12 h (t-CNCs) at a concentration of 0.5 mg/mL. Neat MCC-suspensions as well as MCC/PVOH-mixtures were prepared the same way as aqueous dispersions of MCC and PVOH used for the preparation of m-CNC aerogels and then diluted with H_2O to a concentration of 1 mg/mL. For all CNCs as well as MCC, two drops of the respective suspension were placed on a carbon film on a 200 square mesh copper grid (Electron Microscopy Science, Hatfield, USA) and dried on a tissue paper for at least 6 h. MFC was dispersed in water by stirring for 4 h and subsequent sonication for 4 h, the concentration was 0.1 mg/mL. After transferring one drop of the suspension onto a TEM-grid, drying was done on an aluminum plate at 70°C for at least 3 h. All micrographs were recorded on a Philips CM 100 microscope that was operated with an acceleration voltage of 80 kV.

Density

The density of the nanocellulose/PVOH aerogels was determined by dividing the mass of the aerogels, which was measured on a Mettler Toledo XS3DU balance, by their volume. The volume was determined by measuring the height and diameter of aerogels and calculating the volume assuming the aerogels all have perfect cylindrical shapes. Results reported in Figure 1 and Supporting Information Table S1 are average values of at least three different samples.

Shrinkage

The shrinkage of the nanocellulose/PVOH aerogels relative to the aqueous mixtures from which they were prepared was measured by dividing the diameter of aerogels through the inner diameter of the vials that served as molds and multiplying the result with 100% to express the final value as residual diameter in % of the original diameter. Vertical shrinking could not be determined because the height of samples was determined upon sanding the surfaces and therefore these results do not reflect the real height of aerogels. Results reported in Table I are average values of at least three different samples ± standard deviation.

Mechanical Properties

The mechanical properties of the nanocellulose/PVOH aerogels were measured on a Zwick/Roell Z10 instrument using a load cell with a nominal force of 0.8 N–200 N and parallel plate compression plates. Compression testing was performed, where the samples were compressed and the compressive stress was measured as a function of the compressive strain, using a preload force of 0.5 kPa. Before compression testing, the cylindrical samples were sanded on both faces to obtain samples with a

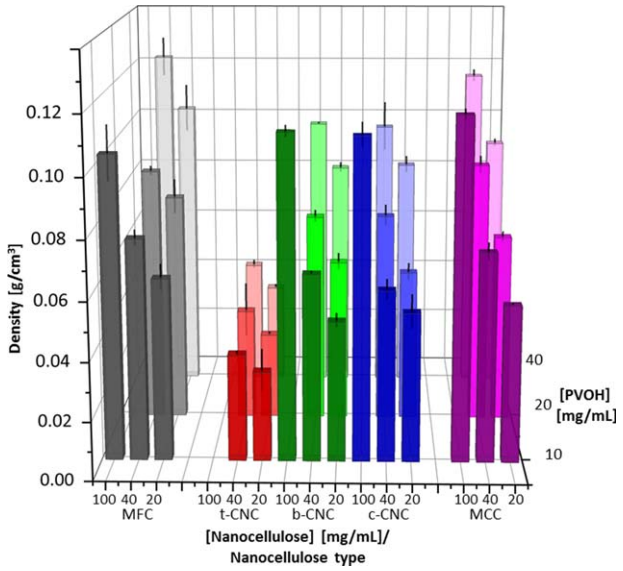

Figure 1. Density of nanocellulose/PVOH aerogels produced from different nanocellulose types as function of nanocellulose and PVOH content in the aqueous mixtures used to prepare the aerogels. All samples were prepared by lyophilizing samples that were slow-frozen (SF) at −26°C for 24 h. [Color figure can be viewed in the online issue, which is available at wileyonlinelibrary.com.]

height of 8–13 mm and a diameter of 12–15 mm. From the resulting stress–strain curves, compressive Young's moduli were determined by measuring the slope at the linear elastic region, typically between 1 and 12% strain, depending on the quality and characteristics of the samples.

RESULTS AND DISCUSSION

Nanocelluloses Used

To probe the dimensions and the structure of the different nanocellulose types used here, TEM-micrographs were acquired of all samples (Supporting Information Figure S1). The images reveal the expected structures and aspect ratios for all nano- and microcelluloses, i.e., well-dispersed whisker-like rods with increasing aspect ratio for cellulose nanocrystals derived from cotton (c-CNCs), cellulose nanocrystals derived from the pseudostem of banana plants (b-CNCs), and cellulose nanocrystals derived from tunicates (t-CNCs), and entangled networks for MFC. The images of ultrasonicated aqueous mixtures of MCC and PVOH (Supporting Information Figure S2) show that the MCC grade used here disintegrates into CNCs (hereafter referred to as m-CNCs, *vide infra*) and not to MFC, as observed previously for polyol-containing MCC-solutions,[61] which is most probably due to the lower PVOH-concentration in the mixtures described in the present work.

Aerogel Preparation

Aerogels made from the different nanocellulose types and PVOH were prepared according to a protocol that was recently described by our group,[46] and is also reminiscent of the procedure reported by Heath *et al.*[14] who, however, did not use PVOH as a polymeric binder. Thus, b-CNCs, t-CNCs, MCC, and MFC were dispersed in aqueous PVOH solutions with a PVOH concentration of [PVOH] = 10, 20 or 40 mg/mL. The nanocellulose concentration [nanocellulose] was set to 20, 40, or 100 mg/mL. Subsequent solvent removal was achieved by freezing and lyophilizing the samples, which resulted in coherent aerogels of the same shape as the mold they were prepared in. Since t-CNCs could not be directly dispersed in PVOH solutions at these high concentrations, t-CNC dispersions were prepared with lower [CNC] and [PVOH] and the concentration was then increased to the desired level through controlled solvent evaporation. We note that this process may lead to a larger error with respect to the composition than in the other systems, and due to the high viscosity of the resulting mixtures it was not possible to prepare aerogels with [t-CNC] = 100 mg/mL, chemical cross-linking with sodium tetraborate could neither be done. We also point out that aggregation of t-CNCs and PVOH was observed for high CNC- and PVOH concentrations and on account of the high viscosity, the formation of bubbles inside the aerogels could not be avoided. The dispersion of MCC in aqueous PVOH solutions was achieved by a combination of mechanical stirring and subsequent sonication. In the case of samples prepared at low PVOH concentrations, the TEM images (see Supporting Information Figure S2) revealed well-separated m-CNCs as already observed previously for ultrasonicated aqueous MCC.[62] Their dimensions (l = 278 ± 60 nm, d = 24 ± 7 nm, A = 11) are comparable with those of c-CNCs. At higher PVOH concentration, aggregation becomes more pronounced (Figure S2c) but it appears that the aggregates have their origin rather in aggregation of m-CNCs induced by PVOH than incomplete disintegration of the MCC.

Building on previous studies performed by the group of Ragauskas[47,48] and our previous work,[46] which all had shown that different freezing rates lead to different pore structures, samples were prepared for lyophilization by freezing them according to two different protocols, either by submersion in liquid nitrogen at −196°C for 5 min (referred to as FF for fast freezing) or storage in a freezer at −26°C for 24 h (referred as SF, slow freezing). Since our previous study revealed better mechanical properties for SF aerogels,[46] we focus the present discussion on this process and the results quoted correspond to SF aerogels unless stated otherwise. As in our previous study, the aerogels were characterized in the as prepared form, and also after thermal annealing or chemically cross-linking with sodium tetraborate ($Na_2B_4O_7$).[46] In a comparative manner, we explored the shrinkage upon lyophilization, thermal annealing or chemical cross-linking, the density, the mechanical properties, and the morphology of all samples.

Shrinkage

The shrinkage of the nanocellulose/PVOH aerogels compared with the aqueous mixtures from which they were prepared was measured by comparing the diameter of the aerogels with the dimensions of the mold in which they had been made and expressing the result as the residual diameter in % of the diameter of the mold, which is considered as their original diameter. Results are shown in Table I. By and large, all samples show little shrinkage and retain between ca. 80 and 95% of their original diameter. The freezing method had no influence on the shrinking behavior, as reflected by the fact that the values for shrinking of SF and FF aerogels were all within the same range.

Table I. Residual Diameter in % of Nanocellulose/PVOH Aerogels as a Function of Their Composition and Freezing Conditions

	Shrinking behavior of nanocellulose/PVOH aerogels				
	Nanocellulose type				
Sample	c-CNC[a]	b-CNC	t-CNC	MFC	MCC
20/10 SF	Cracking	Cracking	94 ± 1	Cracking	Cracking
20/10 FF	84 ± 3	87 ± 2	94 ± 2	81 ± 1	83 ± 2
20/20 SF	86 ± 1	86 ± 1	96 ± 0.5	81 ± 2	77 ± 2
20/20 FF	90 ± 1	89 ± 1	95 ± 1	87 ± 1	85 ± 1
20/40 SF	85 ± 1	85 ± 2	94 ± 1.	84 ± 2	81 ± 1
20/40 FF	79 ± 2	89 ± 1	93 ± 1	86 ± 1	82 ± 1
40/10 SF	85 ± 3	87 ± 1	96 ± 2	76 ± 2	80 ± 2
40/10 FF	93 ± 0.5	92 ± 1	94 ± 1	90 ± 2	89 ± 1
40/20 SF	89 ± 10	89 ± 1	95 ± 1	84 ± 2	80 ± 1
40/20 FF	93 ± 0.5	93 ± 1	94 ± 1	86 ± 1	90 ± 1
40/40 SF	90 ± 3	89 ± 1	96 ± 1	87 ± 2	83 ± 1
40/40 FF	90 ± 1	92 ± 1	96 ± 1	87 ± 1	85 ± 1
20/10 AN	89 ± 2	84 ± 2	94 ± 1	79 ± 1	84 ± 1
20/20 AN	88 ± 1	82 ± 1	92 ± 1	77 ± 1	81 ± 2
20/40 AN	80 ± 2	77 ± 1	92 ± 2	71 ± 1	74 ± 1
40/10 AN	93 ± 1	93 ± 1	96 ± 2	89 ± 3	88 ± 2
40/20 AN	89 ± 3	90 ± 1	92 ± 2	86 ± 1	87 ± 1
40/40 AN	87 ± 2	89 ± 1	96 ± 1	80 ± 1	78 ± 1
40/10 BO	94 ± 2	91 ± 1	n.a.	88 ± 3	91 ± 1
40/20 BO	94 ± 1	89 ± 1	n.a.	85 ± 1	86 ± 1
40/40 BO	92 ± 1	87 ± 1	n.a.	84 ± 2	86 ± 1
100/10 SF	91 ± 10	93 ± 3	n.a.	95 ± 1	95 ± 1
100/10 FF	86 ± 12	88 ± 3	n.a.	92 ± 1	88 ± 2

Sample coding (first column) is as follows: The numbers indicate the concentrations of CNC (10–100 mg/mL) and PVOH (10–40 mg/mL); SF indicates slow (−26°C for 24 h), FF fast freezing (−196°C for 5 min); BO indicates cross-linking with $Na_2B_4O_7$, whereas AN designates thermally annealed samples.

n.a. = not available; these samples could not be prepared due to the high viscosity of t-CNC suspensions. Data represent averages of *N* = at least three independent measurements ± standard deviation.

[a] Results for c-CNC aerogels are reproduced from our previous work.[46]

Aerogels made from the different CNCs generally display less shrinkage than the aerogels prepared from MFC; high-aspect ratio t-CNC aerogels shrink the least and MFC aerogels the most, which can be explained with the high crystallinity of t-CNCs, leading to a high modulus and amorphous parts in MFC, leading to a lower modulus. As shown in Table I, the extent of shrinking during freezing and lyophilization also depends on the composition. Interestingly, the residual diameter appears to be little dependent on the solid content or the nanocellulose concentration, but it appears to increase with decreasing [nanocellulose]: [PVOH] ratio. Since pure PVOH aerogels exhibit a much stronger shrinkage, it seems that the addition of CNCs or MFC decreases shrinkage, especially when the stiffness of the nanocellulose employed is high.

Thermal annealing does not have a significant influence on shrinking, regardless of the composition of aerogels. Aerogels made from MFC represent an exception in this context; here an increase of the PVOH concentration led to increased shrinking of MFC aerogels upon thermal annealing. Since both t-CNCs and MFC have a high-aspect ratio, shrinkage during thermal annealing appears again to be related to the modulus of the nanocellulose: the higher the modulus of the nanocellulose, the less the sample shrinks upon annealing. This conclusion is supported by the shrinking behavior of c-CNC, b-CNC, and m-CNC aerogels, which also showed reduced shrinking upon thermal annealing.

Density

The densities of the aerogels were determined by dividing the mass of the samples by their volume, using the assumption that the aerogels possessed perfectly cylindrical shapes. Measured values for the densities of all aerogels are shown in the Supporting Information Table S1. The densities ranged from 0.03 g/cm^3 for 20/10 and 20/20 aerogels (both SF and FF samples) made from t-CNCs to 0.16 g/cm^3 for 40/40 AN aerogels made from MFC. Figure 1 shows the density of SF aerogels as a function of the composition. Higher solid contents within the aerogels lead to higher densities, as could be expected. However, the density is also reflected in the extent of

Table II. Compressive Young's Modulus in MPa of Nanocellulose/PVOH Aerogels as a Function of Their Composition and Freezing Conditions

	Compressive Young's modulus of nanocellulose/PVOH aerogels				
	Nanocellulose type				
Sample	c-CNC[a]	b-CNC	t-CNC	MFC	MCC
20/10 SF	0.37 ± 0.09	0.41 ± 0.11	1.51 ± 1.28	0.23 ± 0.06	0.18 ± 0.01
20/10 FF	Cracking	Cracking	0.24 ± 0.11	Cracking	Cracking
20/20 SF	0.80 ± 0.32	1.37 ± 0.29	2.05 ± 0.20	0.86 ± 0.16	0.58 ± 0.13
20/20 FF	0.18 ± 0.01	0.21 ± 0.07	1.04 ± 0.13	0.15 ± 0.01	0.10 ± 0.02
20/40 SF	2.89 ± 0.62	3.65 ± 0.67	2.04 ± 0.43	3.40 ± 0.56	3.01 ± 0.76
20/40 FF	1.12 ± 0.34	1.60 ± 0.08	1.48 ± 0.27	1.16 ± 0.43	0.87 ± 0.15
40/10 SF	0.70 ± 0.12	1.18 ± 0.21	3.52 ± 1.96	0.66 ± 0.19	0.37 ± 0.08
40/10 FF	0.15 ± 0.02	0.22 ± 0.03	0.55 ± 0.20	0.17 ± 0.05	0.09 ± 0.04
40/20 SF	1.64 ± 0.32	2.30 ± 0.63	1.3 ± 0.63	1.48 ± 0.24	1.48 ± 0.19
40/20 FF	0.84 ± 0.20	0.62 ± 0.13	0.87 ± 0.47	0.41 ± 0.07	0.18 ± 0.01
40/40 SF	4.16 ± 1.16	5.15 ± 1.84	6.68 ± 0.79	6.67 ± 1.20	5.12 ± 0.21
40/40 FF	1.59 ± 0.34	1.67 ± 0.40	3.91 ± 1.21	1.70 ± 0.40	1.56 ± 0.07
20/10 AN	0.19 ± 0.02	0.28 ± 0.03	0.89 ± 0.29	0.34 ± 0.11	0.25 ± 0.02
20/20 AN	1.11 ± 0.78	1.58 ± 0.34	0.76 ± 0.15	1.88 ± 0.40	0.84 ± 0.22
20/40 AN	3.14 ± 1.58	6.35 ± 1.35	2.13 ± 1.04	15.9 ± 3.52	6.63 ± 1.59
40/10 AN	0.51 ± 0.09	0.49 ± 0.04	3.60 ± 0.31	0.66 ± 0.07	0.55 ± 0.08
40/20 AN	2.04 ± 0.09	2.25 ± 0.41	1.48 ± 0.93	1.93 ± 0.31	1.70 ± 0.21
40/40 AN	5.86 ± 2.07	13.4 ± 2.63	3.59 ± 0.68	9.19 ± 4.74	8.24 ± 1.95
40/10 BO	0.33 ± 0.08	0.20 ± 0.09	n.a.	0.85 ± 0.33	0.55 ± 0.13
40/20 BO	2.28 ± 0.38	1.22 ± 0.49	n.a.	2.10 ± 0.37	1.58 ± 0.48
40/40 BO	7.80 ± 0.89	12.9 ± 2.70	n.a.	16.8 ± 2.14	15.7 ± 3.11
100/10 SF	1.48 ± 0.48	1.07 ± 0.11	n.a.	1.72 ± 0.18	1.09 ± 0.34
100/10 FF	0.62 ± 0.31	0.04 ± 0.01	n.a.	0.50 ± 0.01	0.29 ± 0.06

Sample coding (first column) is as follows: The numbers indicate the concentrations of CNC (10–100 mg/mL) and PVOH (10–40 mg/mL); SF indicates slow (−26°C for 24 h), FF fast freezing (−196°C for 5 min); BO indicates cross-linking with $Na_2B_4O_7$, whereas AN designates thermally annealed samples.

n.a. = not available; these samples could not be prepared due to the high viscosity of t-CNC suspensions. Data represent averages of *N* = at least three independent measurements ± standard deviation.

[a] Results for c-CNC aerogels are reproduced from our previous work.[46]

shrinking, i.e., the more an aerogel shrank during preparation, the higher its density is. For example t-CNC aerogels did practically not shrink and therefore all of them have a comparatively low density whereas annealed MFC aerogels with high PVOH concentrations all have surprisingly high densities, which can be led back to more pronounced shrinking. Exceptions to this trend are 100/10-aerogels; even if shrinking was modest for these samples, their density is comparatively high because of the high solid content. On the other hand, even if their solid content is lower, the density of 40/40 aerogels is higher than the density of 100/10-aerogels. Thus, the density of aerogels was surprisingly more affected by shrinking than by the solid concentrations *per se*. As already observed for the shrinking behavior, the freezing rate did not have any influence on the density of aerogels because the solid content and shrinking (*vide supra*) both were not affected by the freezing rate.

Mechanical Properties

The mechanical properties of the nanocellulose/PVOH aerogels made were measured by performing compression stress–strain tests. Graphs resulting from these experiments show the typical stress–strain behavior of foams, where an initial linear elastic deformation is followed by a flat region caused by pore breaking, and once all the pores are broken, the slope increases drastically due to compression of the bulk material.[63] Representative curves for very strong and very weak samples are shown in the Supporting Information Figure S3. Compressive Young's moduli were determined from the slopes of the linear elastic deformation regimes of the graphs. Due to severe cracking during freezing and lyophilization, most of the 20/10 FF aerogels, except the ones made from t-CNCs, could not be tested. Results for the compressive Young's moduli of all aerogels measured can be found in Table II.

In all cases, the fast-frozen (FF) aerogels display a lower compressive Young's modulus than their slow-frozen (SF) counterparts. This finding is consistent with our earlier observations and can be explained with the formation of micro cracks the aerogels during the FF and the different morphologies (*vide*

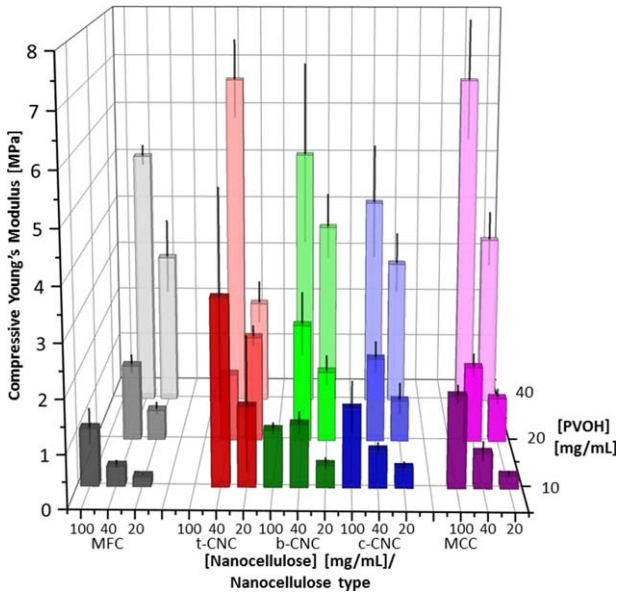

Figure 2. Compressive Young's moduli of nanocellulose/PVOH aerogels produced from different nanocellulose types as function of nanocellulose and PVOH content in the aqueous mixtures used to prepare the aerogels. All samples were prepared by lyophilizing samples that were slow-frozen (SF) at −26°C for 24 h. [Color figure can be viewed in the online issue, which is available at wileyonlinelibrary.com.]

infra).[46] The lowest compressive Young's moduli were observed for the fast-frozen samples prepared from dispersions with a low-solid content and low-aspect ratio CNCs; for example the 20/20 FF aerogels based on c-CNCs, b-CNCs or m-CNCs display a compressive modulus E of ca. 0.1–0.2 MPa, whereas the stiffest samples (40/40 BO made from MFC) exhibit an E of ca. 17 MPa.

A comparison of the compressive moduli of the as-prepared slow-frozen aerogels derived from different nanocellulose types with different CNC concentrations is shown in the diagram in Figure 2. The diagram shows several clear trends. First of all, the observed compressive modulus appears to indeed scale with the aspect ratio of the CNCs, although differences appear to become smaller at high PVOH concentrations.

In particular at low-solid content, aerogels made from t-CNCs exhibit a significantly higher compressive Young's modulus than the other samples, but the measurements unfortunately feature large error bars. The latter can be assigned to microscopic bubbles in the samples, which are formed during preparation and are difficult to remove due to the high viscosity of the t-CNC mixtures, or aggregates formed during the preparation of the dispersions. A further error source might also be the preparation procedure, since the study of aerogels made from t-CNC where the CNC-concentration was determined gravimetrically did not suffer from this problem.[37] The data further show that at least at lower solid content, the aerogels made from longer b-CNCs show a higher compressive modulus than those made from shorter c-CNCs. The latter have properties that are mirrored by aerogels made from m-CNCs, consistent with the comparable dimensions of these two CNC types. The lowest compressive Young's moduli were observed for low-solid-content aerogels made from MFC, which also displays the lowest intrinsic elastic modulus.

In case of the SF aerogels, a twofold increase of the nanocellulose content from 20 mg/mL to 40 mg/mL led to a two-fold increase of the compressive Young's modulus for all aerogel series studied. A further (but less pronounced) stiffness increase was observed when the nanocellulose concentration was increased to 100 mg/mL. Also increasing the PVOH concentration lead to higher compressive Young's moduli in all aerogel series studied. When [PVOH] was increased from 10 mg/mL to 20 mg/mL, the compressive E of aerogels prepared from b-CNCs, c-CNCs, m-CNCs, and MFC increased by a factor of about three, independent of the nanocellulose concentration. The increase of the compressive Young's modulus was more modest when [PVOH] was further increased from 20 mg/mL to 40 mg/mL. Due to the contribution of the semi crystalline PVOH to the overall mechanics, the difference in mechanical properties between aerogels made from the different celluloses decreased with increasing [PVOH]. The relative reinforcement caused by the PVOH binder was much less pronounced for t-CNC aerogels; increasing the PVOH concentration from 10 mg/mL to 20 mg/mL barely caused an increase of the compressive Young's modulus. Increasing the PVOH concentration to 40 mg/mL lead to an increase, but also here much less pronounced than for other nanocelluloses. The reduced influence of the polymeric binder is likely related to the high stiffness and aspect ratio of t-CNCs, leading to high compressive moduli for t-CNC aerogels that barely can be improved through the addition of low amounts of PVOH.

Thermal annealing of the aerogels generally leads to an enhanced compressive Young's modulus. The magnitude of the effect depended on the PVOH content and the type of nanocellulose. At high [PVOH], the difference between the mechanical properties of annealed and as prepared aerogels is by far higher for MFC aerogels than for the other CNC aerogels. This may be related to the shrinking observed in case of these materials, which in turn increases the density and thereby the compressive modulus. Except for t-CNCs, aerogels made from CNCs also undergo shrinking upon thermal annealing if the PVOH-concentration is high. The compressive Young's modulus of the t-CNC aerogels, which are already rather stiff in their as-prepared state, remained almost unchanged upon thermal annealing, while for c-CNCs, m-CNCs and b-CNCs, a significant modulus increase was observed at [PVOH] = 40 mg/mL. The reason for this is not immediately clear but eventually can be led back to the lower elastic modulus and the lower aspect ratio of these CNCs compared with t-CNCs, thus allowing more free moving space for the PVOH during the annealing step. Another explanation is, as mentioned, the rather high stiffness of t-CNC aerogels in the as-prepared state, which barely can be improved upon thermal annealing.

Chemical cross-linking of the nanocellulose aerogels with $Na_2B_4O_7$ lead to enhanced mechanical properties for all types of nanocellulose if the [PVOH] was higher than 10 mg/mL. In the case of materials where [PVOH] = 10 mg/mL, the PVOH

Table III. Specific Compressive Young's Modulus in MPa·cm^3·g^{-1} of Nanocellulose/PVOH Aerogels as a Function of Their Composition and Freezing Conditions

	Specific compressive Young's modulus of nanocellulose/PVOH aerogels				
	Nanocellulose type				
Sample	c-CNC[a]	b-CNC	t-CNC	MFC	MCC
20/10 SF	7.11 ± 0.99	8.54 ± 1.89	43.7 ± 31.1	4.33 ± 1.05	2.89 ± 0.11
20/10 FF	Cracking	Cracking	8.17 ± 3.52	Cracking	Cracking
20/20 SF	14.8 ± 5.31	24.2 ± 4.51	65.7 ± 7.23	13.0 ± 2.09	7.26 ± 1.14
20/20 FF	3.42 ± 0.19	3.62 ± 1.03	35.2 ± 3.21	2.09 ± 0.09	1.51 ± 0.26
20/40 SF	31.3 ± 5.86	44.6 ± 7.49	57.9 ± 10.9	37.2 ± 5.81	28.6 ± 4.95
20/40 FF	12.8 ± 0.23	17.3 ± 0.58	39.8 ± 6.61	11.8 ± 3.97	8.18 ± 1.24
40/10 SF	11.9 ± 1.50	18.4 ± 3.10	95.5 ± 51.2	9.21 ± 2.22	4.92 ± 0.94
40/10 FF	3.03 ± 0.70	3.02 ± 0.31	14.2 ± 4.58	1.60 ± 0.41	0.78 ± 0.10
40/20 SF	22.3 ± 3.36	31.3 ± 7.78	33.8 ± 10.3	16.1 ± 2.27	16.6 ± 1.80
40/20 FF	11.7 ± 3.04	7.69 ± 1.49	23.3 ± 11.3	4.14 ± 0.60	1.77 ± 0.07
40/40 SF	42.4 ± 8.46	52.2 ± 18.5	151 ± 12.8	57.1 ± 9.34	41.5 ± 0.79
40/40 FF	14.3 ± 2.93	15.4 ± 3.29	88.7 ± 23.9	14.6 ± 2.65	12.0 ± 0.44
20/10 AN	4.55 ± 0.35	5.48 ± 0.36	32.1 ± 6.23	5.80 ± 1.62	4.31 ± 0.31
20/20 AN	19.8 ± 13.0	22.1 ± 4.08	24.34 ± 4.35	20.5 ± 3.69	8.15 ± 1.41
20/40 AN	35.6 ± 3.27	51.6 ± 10.3	56.8 ± 25.4	97.9 ± 19.8	47.0 ± 10.0
40/10 AN	9.06 ± 1.36	9.40 ± 0.68	98.1 ± 4.10	9.06 ± 0.60	7.28 ± 0.92
40/20 AN	28.2 ± 0.64	31.7 ± 5.59	37.9 ± 21.1	20.7 ± 2.78	18.1 ± 1.63
40/40 AN	61.1 ± 17.7	169 ± 29.0	74.9 ± 12.9	63.4 ± 31.3	57.4 ± 5.16
40/10 BO	6.48 ± 0.77	4.30 ± 1.69	n.a.	10.7 ± 0.47	10.2 ± 1.19
40/20 BO	26.7 ± 1.71	19.1 ± 7.39	n.a.	25.4 ± 3.95	20.9 ± 3.56
40/40 BO	89.3 ± 4.87	114 ± 20.2	n.a.	164 ± 16.0	159 ± 30.4
100/10 SF	15.7 ± 5.60	9.57 ± 0.84	n.a.	14.8 ± 1.30	9.33 ± 1.86
100/10 FF	4.99 ± 2.21	0.31 ± 0.10	n.a.	4.10 ± 0.04	1.79 ± 0.06

Sample coding (first column) is as follows: The numbers indicate the concentrations of CNC (10–100 mg/mL) and PVOH (10–40 mg/mL); SF indicates slow (−26°C for 24 h), FF fast freezing (−196°C for 5 min); BO indicates cross-linking with $Na_2B_4O_7$, whereas AN designates thermally annealed samples.

n.a. = not available; these samples could not be prepared due to the high viscosity of t-CNC suspensions. Data represent averages of N = at least three independent measurements ± standard deviation.

[a] Results for c-CNC aerogels are reproduced from our previous work.46

concentration was apparently too low to allow for cross-linking. As observed in our previous study,[46] the addition of $Na_2B_4O_7$ did not lead to gel formation in the wet gel but rather caused precipitation of CNCs, which is reflected in a reduction of the compressive Young's modulus of the resulting aerogels compared with as-prepared aerogels having the same composition. Differences between the compressive Young's modulus for as-prepared and chemically cross-linked aerogels with [PVOH] = 20 mg/mL or more follow the same trend as in case of the annealed aerogels; cross-linked aerogels had higher compressive Young's moduli, with the effect more pronounced at higher PVOH-concentrations. For MFC samples the effect of cross-linking on the mechanical properties is more pronounced than for the CNC aerogels, and even at [PVOH] = 10 mg/mL, chemically cross-linked samples show higher compressive Young's moduli than untreated aerogels. Perhaps due to their higher flexibility compared with CNCs, unless CNCs, MFC may be able to participate in the cross-linking with $Na_2B_4O_7$. The participation of MFC in the cross-linking would lead to more cross-links within the aerogel and therewith would explain the increased stiffness.

Specific Mechanical Properties

Because the compressive mechanical properties of aerogels depend, as discussed above, on their solid content, it is often useful to base comparisons on their specific compressive Young's modulus, which is obtained by dividing the compressive Young's modulus by the density.[37] A complete set of the results is shown in Table III. With the exception of annealed aerogels made from [MFC] = 20 mg/mL and [PVOH] = 40 mg/mL, the results obtained for specific compressive Young's moduli follow the same trends as the compressive Young's moduli. The lowest values were again obtained for all 20/20 FF samples, except for t-CNC aerogels, and the highest values were obtained for 40/40 BO aerogels.

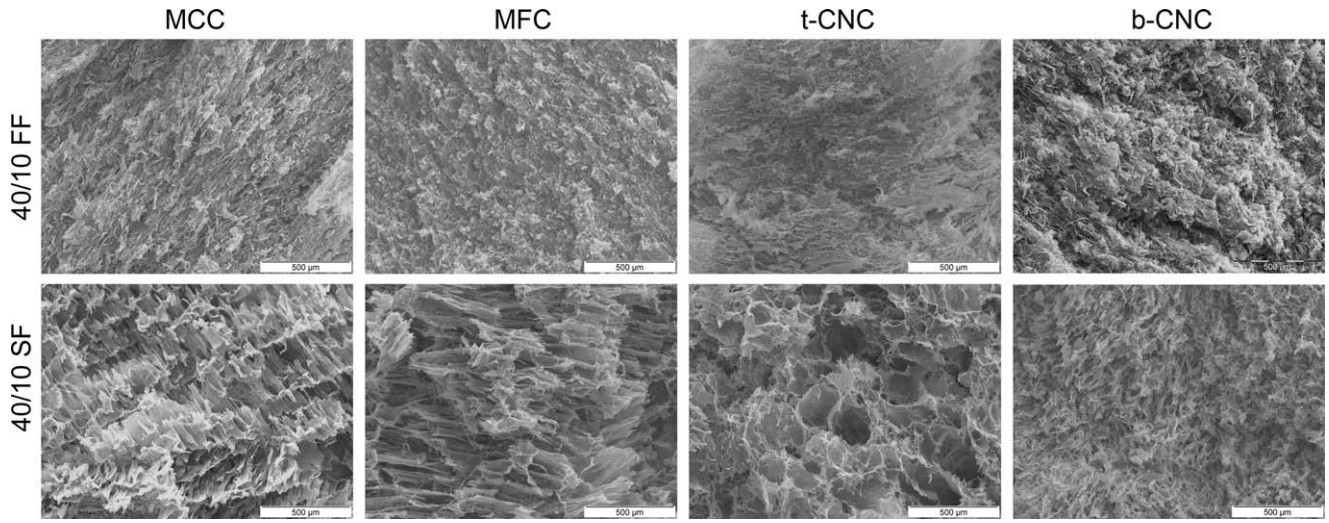

Figure 3. SEM micrographs of nanocellulose/PVOH aerogels prepared from aqueous mixtures with [nanocellulose] = 40 mg/mL and [PVOH] = 10 mg/mL. The aerogels contain MCC, MFC, t-CNC and b-CNC (from left to right). Dispersions were lyophilized after fast freezing (FF, top row) at −196°C for 5 min or slow freezing (SF, bottom row) at −26°C for 24 h. All scale bars represent 500 µm.

20/40 AN aerogels made from MFC have a comparably high specific compressive Young's modulus, but due to the increased density caused by shrinking during thermal annealing this value decreased that of the other aerogels. Variation of the nanocellulose and PVOH concentration influences the specific compressive modulus in a manner that is different from the influence that these concentrations exert on *E*; increasing the nanocellulose concentration did not affect the specific compressive Young's modulus, as the increase in stiffness was largely compensated by the associated increase in density. On the other hand, an increase of the PVOH concentration by a factor of two lead to a two-fold increase of the specific compressive Young's modulus, confirming the previously observed the synergistic effect of PVOH on the mechanical properties of the aerogels.[37,41]

To compare the effect of chemical cross-linking with the effect of the use of high-aspect ratio CNCs on the specific compressive Young's modulus of aerogels, the specific compressive Young's modulus measured for the 40/40 BO aerogels made from MFC was compared with the value of t-CNC aerogels with the identical CNC- and PVOH concentration (40/40 SF). Results showed the same value for both types of aerogels.

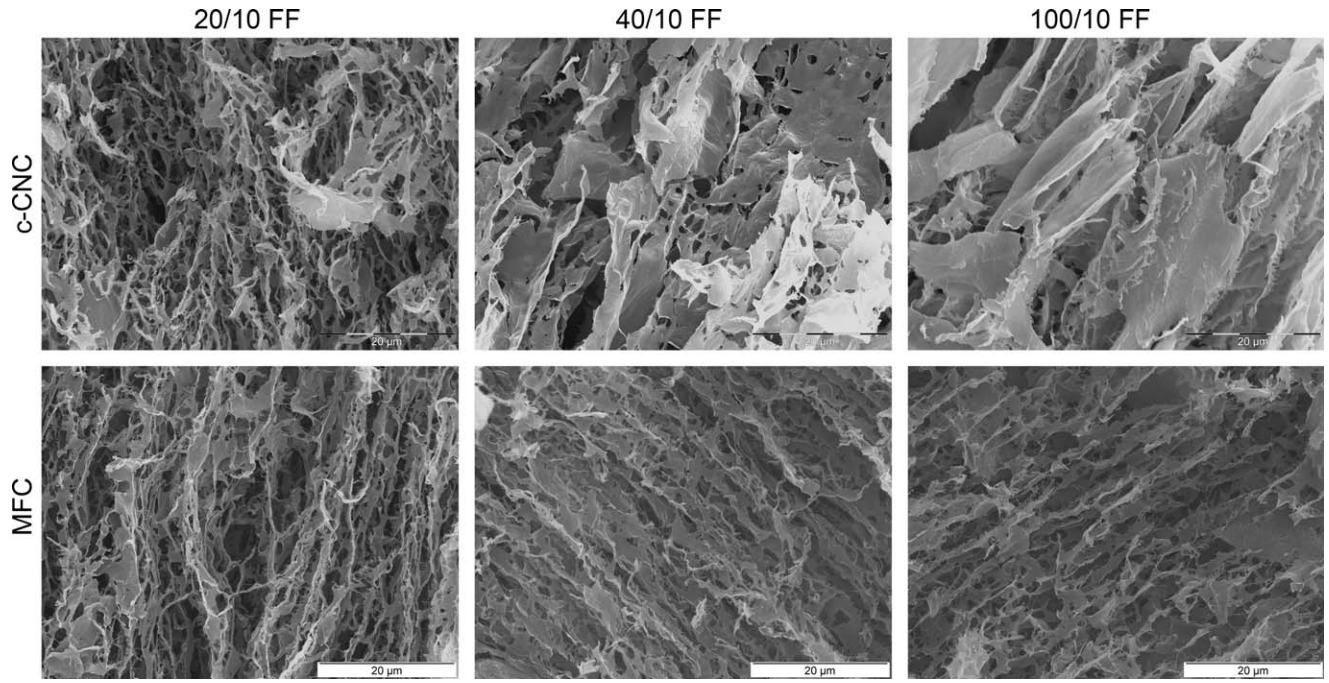

Figure 4. SEM micrographs of nanocellulose/PVOH aerogels made from aqueous dispersions containing MFC or c-CNC with [PVOH] = 10 mg/mL and [nanocellulose] as indicated in the figure. Dispersions were lyophilized after FF at −196°C for 5 min. All scale bars represent 20 µm.

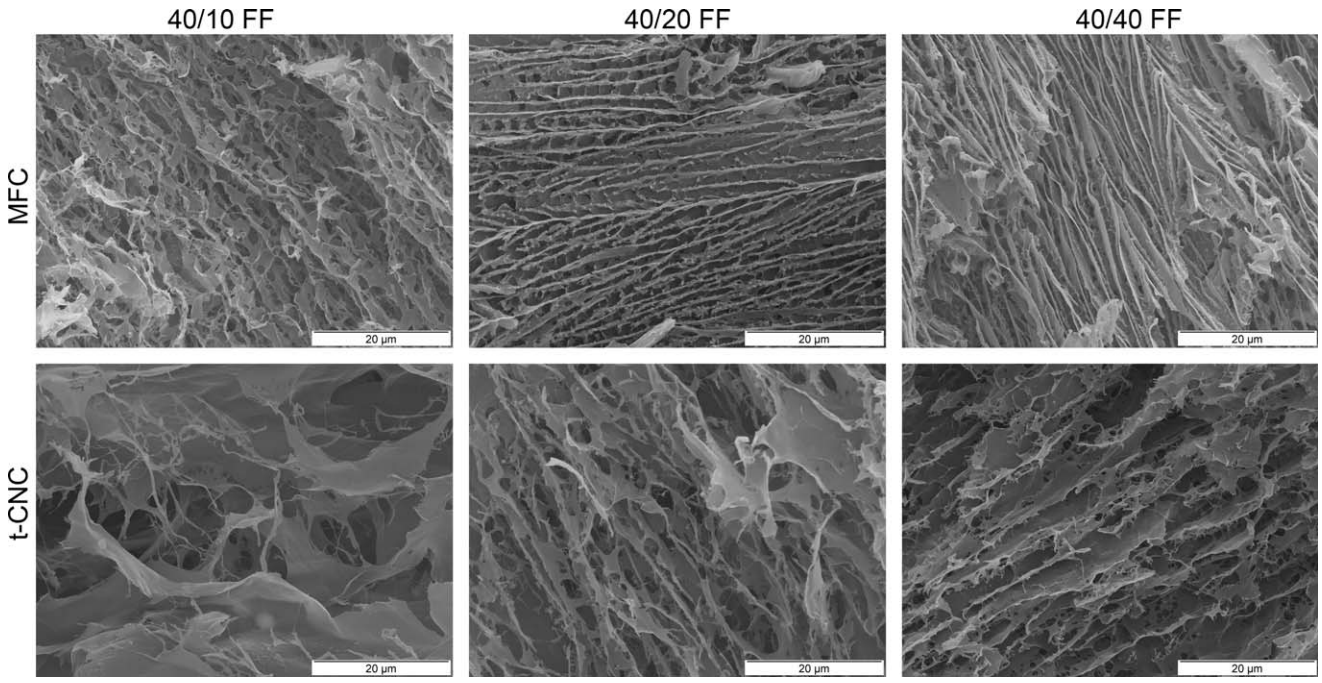

Figure 5. SEM micrographs of aerogels made from t-CNC and MFC with [nanocellulose] = 40 mg/mL, and different [PVOH], as indicated in the figure. Dispersions were lyophilized after FF at −196°C for 5 min.

Hence, at low-solid concentrations, aerogels made from CNCs with a high-aspect ratio and a high elastic modulus lead to aerogels with better mechanical properties. Upon the addition of high amounts of polymeric binder or by adding a cross-linker, this difference between aerogels made from different nanocellulose decreases and the influence of the polymeric binder or the cross-linker, respectively, are predominant and the aspect ratio does not affect the mechanical properties.

Morphology

The morphology of the materials studied was probed by SEM. A comparison of SEM micrographs of FF and SF aerogels (Figure 3) reveals similar morphologies and trends as previously observed for c-CNC aerogels.[46] FF-aerogels exhibit a sheet-like morphology while SF aerogels exhibit a three-dimensional network structure, in which sheets are connected with struts and the average pore size is around 20 µm. Surprisingly, the pore size of t-CNC aerogels is much larger (up to 200 µm) which most probably can be assigned to the different preparation procedure.

As previously observed for c-CNC aerogels, the CNC concentration does not have any effect on the morphology of the SF aerogels, as shown in the Supporting Information Figure S4. For FF aerogels, the trends of the aerogels described here are similar to the one of the c-CNC aerogels,[46] where the structure is lamellar and the pore size is smaller if the CNC-concentration is below 40 mg/mL and similar to the three-dimensional network, where sheets are connected with struts, of SF aerogels, if a high CNC concentration of 100 mg/mL is used. For MFC aerogels, however, this trend does not appear to hold; even if the MFC concentration was as high as 100 mg/mL the pore morphology did not change but remained lamellar with small pores and seems to be governed by ice growth and its interaction with PVOH (Figure 4). Since t-CNC aerogels do not show this behavior while also having also a high-aspect ratio, this can be assigned to the low stiffness of MFC, enabling the ice crystals to grow in the same way as at low nanocellulose-concentrations, since the low stiffness does not lead to a change in viscosity upon adding a larger amount of nanocellulose.

The PVOH-concentration did not have any major influence on the morphology of SF aerogels (see Supporting Information Figure S5) if the nanocellulose concentration was both 20 and 40 mg/mL. For all FF samples, except aerogels made from t-CNCs and MFC, the addition of PVOH did change the morphology of FF aerogels (See Figure 4). Increasing the PVOH concentration leads to a higher extent of fishbone-shaped, arranged structures. This fishbone structure occurs in all aerogels except t-CNC aerogels. The comparatively high stiffness of t-CNCs compared with all other nanocelluloses combined with their high-aspect ratio, thereby decreasing the degrees of freedom of the PVOH-chains due to the high viscosity of the suspensions, seems to be the reason for this different behavior.

As already observed for the shrinking behavior and the mechanical properties, thermal annealing does not influence the morphology of t-CNC aerogels but has an effect on the morphology of MFC- and m-CNC aerogels at high PVOH-concentrations. In Figure 5, SEM-micrographs of annealed and as prepared aerogels made from MFC and t-CNCs with a high PVOH-concentration reveal that thermal annealing of MFC-aerogels leads to smaller pore sizes for annealed aerogels while the overall morphology did not undergo any significant change. On the other hand, thermal annealing of t-CNC-aerogels did not lead to any change in morphology or the pore size. Combining this

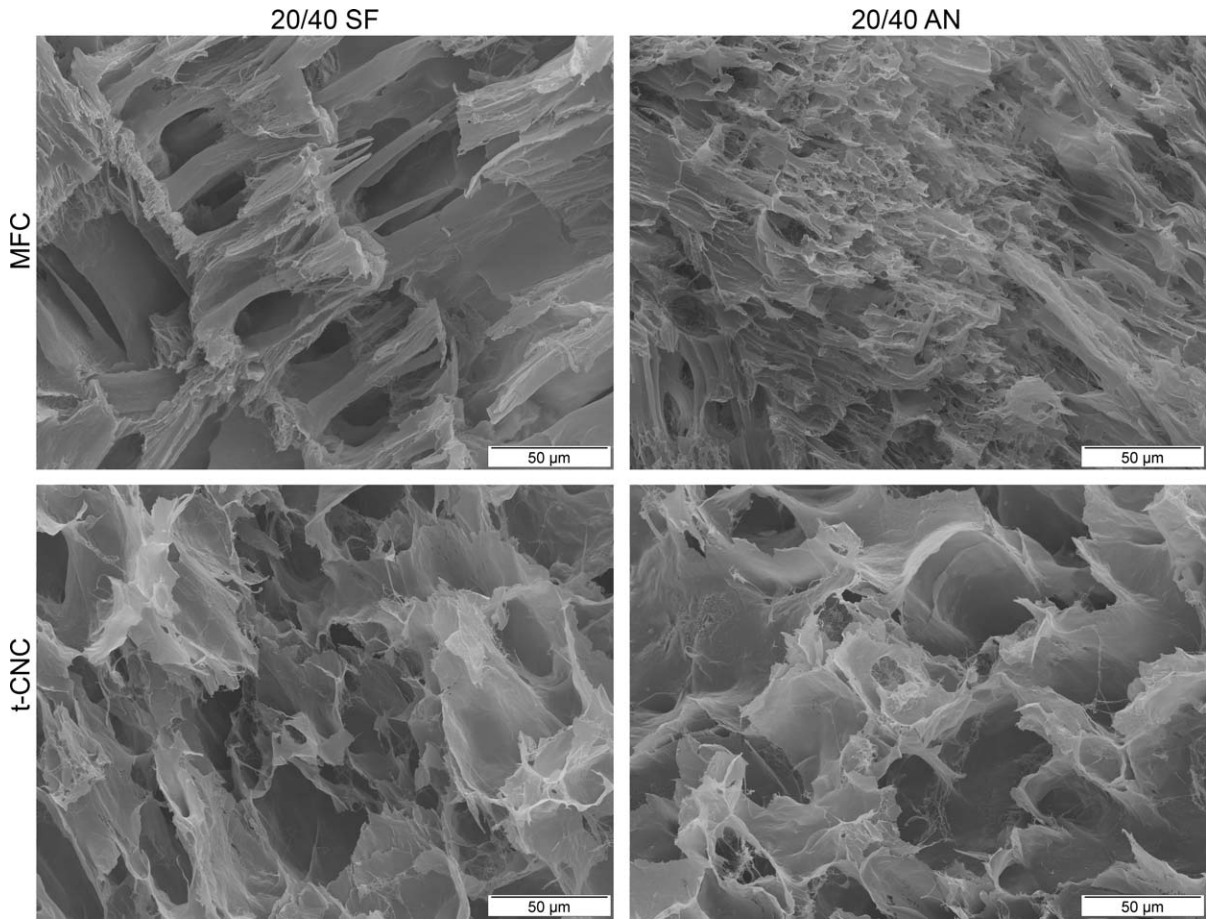

Figure 6. SEM micrographs of t-CNC and MFC-aerogels with [nanocellulose] = 20 mg/mL and [PVOH] = 40 mg/mL. Dispersions were lyophilized after SF at −26°C for 24 h. Aerogels shown in the micrographs on the left side (SF) did not go any further treatment upon freezing and lyophilization whereas aerogels shown in the micrographs on the right side were thermally annealed (AN) after lyophilization.

observation with values obtained for shrinking and densities of aerogels leads to the conclusion that shrinking during thermal annealing leads to a diminished pore size of annealed aerogels.

In accordance with our previous work,[46] chemical cross-linking of nanocellulose/PVOH-aerogels with $Na_2B_4O_7$ leads to smaller pores (see Supporting Information Figure S6). Unlike for the mechanical properties, the effect of chemical cross-linking on the morphology was the same for all kinds of nanocellulose.

CONCLUSIONS

Aerogels made from different types of nanocellulose and PVOH were prepared and their properties were compared with those of previously reported c-CNC/PVOH aerogels having otherwise the same composition. The use of CNCs with a higher aspect ratio, such as t-CNCs suppresses shrinking of aerogels, both during freeze-drying or thermal annealing. Since this effect was not observed for aerogels made from MFC and is neither very pronounced for the other CNC types investigated, it appears that a high-aspect ratio combined with a high elastic modulus of the nanocellulose diminishes shrinking. This is also reflected in the significant lower densities of t-CNC aerogels. If the cellulose content in the aerogels is higher than the PVOH content, higher aspect ratios combined with higher elastic moduli of the nanocellulose also lead to higher compressive Young's moduli. With increasing binder concentration or upon addition of a chemical cross-linker, this effect is suppressed and the mechanical properties of those aerogels appear to be dominated by the semi crystalline PVOH binder. A comparison of the specific compressive Young's moduli of aerogels made from t-CNCs with a high solid concentration and cross-linked aerogels with a high binder content and having the same [CNC] and [PVOH] reveals similar values of around 150 $MPa{\cdot}cm^3{\cdot}g^{-1}$. It further demonstrates that different design approaches can be used to create nanocellulose-based aerogels with high specific compressive moduli.

ACKNOWLEDGMENTS

The authors gratefully acknowledge funding from the Swiss National Science Foundation (National Research Program 64, Project #406440_131264/1 and National Research Program 66, Project #406640_136911) and the Adolphe Merkle Foundation. We thank Christoph Neururer for assistance with the SEM experiments.

REFERENCES

1. Favier, V.; Chanzy, H.; Cavaille, J. Y. *Macromolecules* **1995**, *28*, 6365.

2. Schroers, M.; Kokil, A.; Weder, C. *J. Appl. Polym. Sci* **2004**, *93*, 2883.
3. Zimmermann, T.; Pöhler, E.; Geiger, T. *Adv. Eng. Mater* **2004**, *6*, 754.
4. Lu, J.; Wang, T.; Drzal, L. T. *Compos. Part A: Appl. Sci. Manuf.* **2008**, *39*, 738.
5. Tang, L.; Weder, C. *ACS Appl. Mater. Interface* **2010**, *2*, 1073.
6. Mendez, J.; Annamalai, P. K.; Eichhorn, S. J.; Rusli, R.; Rowan, S. J.; Foster, E. J.; Weder, C. *Macromolecules* **2011**, *44*, 6827.
7. Kumar, S.; Hofmann, M.; Steinmann, B.; Foster, E. J.; Weder, C. *ACS Appl. Mater. Interfaces* **2012**, *4*, 5399.
8. Kumar, V.; Bollström, R.; Yang, A.; Chen, Q.; Chen, G.; Salminen, P.; Bousfield, D.; Toivakka, M. *Cellulose* 2014, 1.
9. Aulin, C.; Netrval, J.; Wagberg, L.; Lindstrom, T. *Soft Matter* **2010**, *6*, 3298.
10. Cervin, N.; Aulin, C.; Larsson, P.; Wågberg, L. *Cellulose* 2012, *19*, 401.
11. Korhonen, J. T.; Kettunen, M.; Ras, R. H. A.; Ikkala, O. *ACS Appl. Mater. Interface* **2011**, *3*, 1813.
12. Minelli, M.; Baschetti, M. G.; Doghieri, F.; Ankerfors, M.; Lindström, T.; Siró, I.; Plackett, D. *J. Membr. Sci.* **2010**, *358*, 67.
13. Pääkkö, M.; Vapaavuori, J.; Silvennoinen, R.; Kosonen, H.; Ankerfors, M.; Lindstrom, T.; Berglund, L. A.; Ikkala, O. *Soft Matter* **2008**, *4*, 2492.
14. Heath, L.; Thielemans, W. *Green Chem.* **2010**, *12*, 1448.
15. Heath, L.; Zhu, L.; Thielemans, W. *ChemSusChem.* **2013**, *6*, 537.
16. Habibi,; Y,; Lucia,; L. A. Polysaccharide Building Blocks, A sustainable Approach to the Development of Renewable Biomaterials; John Wiley & Sons:Hoboken, New Jersey, **2012**.
17. Koga, H.; Azetsu, A.; Tokunaga, E.; Saito, T.; Isogai, A.; Kitaoka, T. *J. Mater. Chem.* **2012**, *22*, 5538.
18. Carlsson, D. O.; Nystrom, G.; Zhou, Q.; Berglund, L. A.; Nyholm, L.; Stromme, M. *J. Mater. Chem.* **2012**, *22*, 19014.
19. Liang, H.-W.; Guan, Q.-F.; Zhu, Z.; Song, L.-T.; Yao, H.-B.; Lei, X.; Yu, S.-H. *NPG Asia Mater.* **2012**, *4*, e19.
20. Jin, H.; Kettunen, M.; Laiho, A.; Pynnönen, H.; Paltakari, J.; Marmur, A.; Ikkala, O.; Ras, R. H. A. *Langmuir* **2011**, *27*, 1930.
21. Zhang, Z.; Sèbe, G.; Rentsch, D.; Zimmermann, T.; Tingaut, P. *Chem. Mater.* **2014**, *26*, 2659.
22. Gao, K.; Shao, Z.; Li, J.; Wang, X.; Peng, X.; Wang, W.; Wang, F. *J. Mater. Chem. A* **2013**, *1*, 63.
23. Faivre, D. *Nat. Nanotechnol.* **2010**, *5*, 562.
24. Olsson, R. T.; Azizi Samir, M. A. S.; Salazar Alvarez, G.; Belova, L.; Strom, V.; Berglund, L. A.; Ikkala, O.; Nogues, J.; Gedde, U. W. *Nat. Nanotechnol.* **2010**, *5*, 584.
25. Valo, H.; Arola, S.; Laaksonen, P.; Torkkeli, M.; Peltonen, L.; Linder, M. B.; Serimaa, R.; Kuga, S.; Hirvonen, J.; Laaksonen, T. *Eur. J. Pharm. Sci.* **2013**, *50*, 69.
26. Haimer, E.; Wendland, M.; Schlufter, K.; Frankenfeld, K.; Miethe, P.; Potthast, A.; Rosenau, T.; Liebner, F. *Macromol. Symp.* **2010**, *294*, 64.
27. Bodin, A.; Concaro, S.; Brittberg, M.; Gatenholm, P. *J. Tissue Eng. Regen. Med.* **2007**, *1*, 406.
28. Sehaqui, H.; Salajkova, M.; Zhou, Q.; Berglund, L. A. *Soft Matter* **2010**, *6*, 1824.
29. Sehaqui, H.; Zhou, Q.; Berglund, L. A. *Compos. Sci. Technol.* **2011**, *71*, 1593.
30. Sehaqui, H.; Zhou, Q.; Ikkala, O.; Berglund, L. A. *Biomacromolecules* **2011**, *12*, 3638.
31. Liebner, F.; Haimer, E.; Wendland, M.; Neouze, M.-A.; Schlufter, K.; Miethe, P.; Heinze, T.; Potthast, A.; Rosenau, T. *Macromol. Biosci.* **2010**, *10*, 349.
32. Rosenau, T.; Potthast, A.; Liebner, F.; Ebner, G.; Renfrew, A. H.; Eichhorn, S.; Fürst-Wiesmann, E.-B. *Cellulose* **2009**, *16*, 929.
33. Bodin, A.; Bäckdahl, H.; Fink, H.; Gustafsson, L.; Risberg, B.; Gatenholm, P. *Biotechnol. Bioeng.* **2007**, *97*, 425.
34. Sescousse, R.; Gavillon, R.; Budtova, T. *Carbohydr. Polym.* **2011**, *83*, 1766.
35. Duchemin, B. J. C.; Staiger, M. P.; Tucker, N.; Newman, R. H. *J. Appl. Polym. Sci.* **2010**, *115*, 216.
36. Surapolchai, W.; Schiraldi, D. *Polym. Bull* **2010**, *65*, 951.
37. Gawryla, M. D.; van den Berg, O.; Weder, C.; Schiraldi, D. A. *J. Mater. Chem.* **2009**, *19*, 2118.
38. Li, Y.; Ren, H.; Ragauskas, A. J. *J. Nanosci. Nanotechnol.* **2011**, *11*, 6904.
39. Uraki, Y.; Nemoto, J.; Otsuka, H.; Tamai, Y.; Sugiyama, J.; Kishimoto, T.; Ubukata, M.; Yabu, H.; Tanaka, M.; Shimomura, M. *Carbohydr. Polym.* **2007**, *69*, 1.
40. Zhang, J.; Cao, Y.; Feng, J.; Wu, P. *J. Phys. Chem. C* **2012**, *116*, 8063.
41. Javadi, A.; Zheng, Q.; Payen, F.; Javadi, A.; Altin, Y.; Cai, Z.; Sabo, R.; Gong, S. *ACS Appl. Mater. Interfaces* **2013**, *5*, 5969.
42. Zheng, Q.; Cai, Z.; Gong, S. *J. Mater. Chem. A* **2014**, *2*, 3110.
43. Dufresne, A. *J. Nanosci. Nanotechnol.* **2006**, *6*, 322.
44. Bras, J.; Viet, D.; Bruzzese, C.; Dufresne, A. *Carbohydr. Polym.* **2011**, *84*, 211.
45. Takayanagi, M.; Uemura, S.; Minami, S. *J. Polym. Sci. Part C: Polym. Symp.* **1964**, *5*, 113.
46. Mueller, S.; Weder, C.; Foster, E. J. *Green Mater.* **2014**, *2*, 169.
47. Dash, R.; Li, Y.; Ragauskas, A. J. *Carbohydr. Polym.* **2012**, *88*, 789.
48. Zhou, Y.; Fu, S.; Pu, Y.; Pan, S.; Levit, M. V.; Ragauskas, A. J. *RSC Adv.* **2013**, *3*, 19272.
49. Ochiai, H.; Fukushima, S.; Fujikawa, M.; Yamamura, H. *Polym. J* **1976**, *8*, 131.
50. Ochiai, H.; Shimizu, S.; Tadokoro, Y.; Murakami, I. *Polymer* **1981**, *22*, 1456.
51. Siró, I.; Plackett, D. *Cellulose* **2010**, *17*, 459.
52. Rusli, R.; Eichhorn, S. J. *Appl. Phys. Lett.* **2008**, *93*, 033111.

53. Šturcová, A.; Davies, G. R.; Eichhorn, S. J. *Biomacromolecules* **2005**, *6*, 1055.
54. Aulin, C.; Ahola, S.; Josefsson, P.; Nishino, T.; Hirose, Y.; Österberg, M.; Wågberg, L. *Langmuir* **2009**, *25*, 7675.
55. Johar, N.; Ahmad, I.; Dufresne, A. *Ind. Crops Prod.* **2012**, *37*, 93.
56. Siquiera, G.; Bras, J.; Dufresne, A. *BioResources* **2010**, *5*, 14.
57. Bledzki, A. K.; Gassan, J. *Prog. Polym. Sci.* **1999**, *24*, 221.
58. Mueller, S.; Weder, C.; Foster, E. J. *RSC Adv.* **2014**, *4*, 907.
59. Shanmuganathan, K.; Capadona, J. R.; Rowan, S. J.; Weder, C. *ACS Appl. Mater. Interfaces* **2009**, *2*, 165.
60. Josset, S.; Orsolini, P.; Siquiera, G.; Tejado, A.; Tingaut, P.; Zimmermann, T. *Nordic Pulp Paper Res. J* **2014**, *29*, 167.
61. Bandera, D.; Sapkota, J.; Josset, S.; Weder, C.; Tingaut, P.; Gao, X.; Foster, E. J.; Zimmermann, T. *React. Funct. Polym.* *85*, 134.
62. Capadona, J. R.; Shanmuganathan, K.; Trittschuh, S.; Seidel, S.; Rowan, S. J.; Weder, C. *Biomacromolecules* **2009**, *10*, 712.
63. Gibson,; L. J.; Ashby,; M. F. Cellular Solids-Structure and properties; Press Syndicate of the University of Cambridge:, **1997**.